

Article

Dihalogen and Pnictogen Bonding in Crystalline Icosahedral Phosphaboranes

 Jindřich Fanfrlík ^{1,*}  and Drahomír Hnyk ^{2,*}
¹ Institute of Organic Chemistry and Biochemistry of the Czech Academy of Sciences, Flemingovo nam. 2, 16610 Prague 6, Czech Republic

² Institute of Inorganic Chemistry of the Czech Academy of Sciences, 25068 Husinec-Řež, Czech Republic

* Correspondence: fanfrlik@uochb.cas.cz (J.F.); hnyk@iic.cas.cz (D.H.)

Received: 6 September 2018; Accepted: 9 October 2018; Published: 13 October 2018



Abstract: Noncovalent interactions in the single crystal of 3,6-Cl₂-*closo*-1,2-P₂B₁₀H₈ and in the crystal of *closo*-1,7-P₂B₁₀Cl₁₀•toluene were analyzed by means of quantum chemical computations. The crystal packing in the second crystal was dominated by numerous B-Cl⋯Cl-B dihalogen and strong B-P⋯π pnictogen bonds, the latter of which were characterized by a small length of 3.08 Å and a large interaction energy value, exceeding −10 kcal mol^{−1}.

Keywords: sigma hole; heteroborane; co-crystal

1. Introduction

Phosphorus atoms can be relatively easily incorporated into the icosahedral *closo*-B₁₂H₁₂^{2−} skeleton, which is achieved experimentally by reacting a boron hydride with an open pentagonal belt, e.g. B₁₀H₁₄, with PCl₃ [1,2]. Such a reaction yields *closo*-1,2-P₂B₁₀H₁₀ and its mono- and di-chloro derivatives. Among them, 3,6-Cl₂-*closo*-1,2-P₂B₁₀H₈ (**1**) has been crystallized after separation from the reaction mixture. The parent phosphaborane can be thermally rearranged to obtain the isomeric *closo*-1,7-P₂B₁₀H₁₀ [3]. However, when the pyrolysis reaction of B₂Cl₄ with PCl₃ takes place, the terminal hydrogens of the latter cage are completely substituted by chlorines, resulting in *closo*-1,7-P₂B₁₀Cl₁₀ (**2**). The molecular diagrams of **1** and **2** with numbering are shown in Figure 1. Compound **2** is prone to crystallization with toluene, yielding crystals of **2**•C₆H₅CH₃ in this process [4].

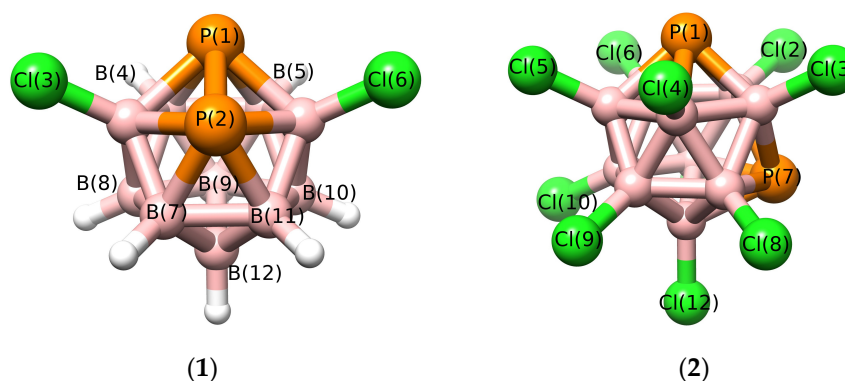


Figure 1. The molecular diagrams and numbering of 3,6-Cl₂-*closo*-1,2-P₂B₁₀H₈ (**1**) and *closo*-1,7-P₂B₁₀Cl₁₀ (**2**).

The phosphorus atoms of *closo*-1,2-P₂B₁₀H₁₀ and *closo*-1,7-P₂B₁₀H₁₀ are incorporated into the skeleton via multicenter 3-center-2-electron (3c2e) and 4-center-2-electron (4c2e) types of bonding [5].

The electron distribution is in disagreement with the classical electronegativity concept in multicenter bonding [5,6] and it results in areas of highly positive electrostatic potential, called σ -holes [7], on phosphorus atoms [8]. The concept of σ -hole, developed by Politzer et al., was originally used to describe halogen (X) bonds, where the σ -hole was centered on the carbon–halogen σ -bond axis. A partially positive σ -hole on a partially negative X atom could thus explain the interesting ability of an X atom to interact simultaneously with electrophiles and nucleophiles.

Closo-phosphaboranes are not the only heteroboranes with highly positive σ -holes. Indeed, various chalcogen and X-bonds have been reported for *closo*-thiaboranes and halogenated carboranes [9–11]. In addition, pnictogen (Pn) bonds are known for various *nido*- $\text{Pn}_2\text{C}_2\text{B}_7\text{H}_n\text{X}_{9-n}$ (Pn = P, As, Sb) molecules [12,13]. All these σ -hole interactions have been reported for single crystalline materials. In order to expand the body of Pn-bonding in *closo* structural motifs, we have selected a known crystal structure of **1** [1]. Additionally, we selected the crystal of **2** cocrystallized with toluene [4] for quantum chemical analysis, the first candidate for a non-single-crystalline material in boron cluster chemistry stabilized by σ -hole interactions.

2. Materials and Methods

The molecular electrostatic potential (ESP) surfaces of isolated molecules **1** and **2** were computed at the Hartree-Fock (HF) level with the correlation-consistent polarized valence double-zeta (cc-pVDZ) basis set using the Gaussian09 [14] and Molekel4.3 [15,16] programs. As a one-electron property, ESP is correctly described by the non-correlated HF method and the double-zeta basis set size is sufficient for its computation [17].

Around each unique molecule in the studied crystals, we created clusters by considering the surrounding molecules. The molecules that had any atom within 5 Å of the central molecule formed a cluster that was called the first layer. The second layer was obtained by considering molecules that had any atom within 5 Å of the first layer. Hydrogen atoms in the central molecule and in the first layer were optimized using the density functional theory (DFT) with the resolution of identity (RI) approximation, the empirical dispersion (D3), the Becke, Lee, Yang and Parr functional (BLYP), and the double-zeta valence polarized (DZVP) basis set [18]. Hydrogen atoms of the second layer were optimized by the hybrid DFT-D3/PM6-D3H4X approach. The DFT-D3/BLYP/DZVP method was used for the first layer and the corrected semiempirical quantum mechanical PM6-D3H4X method [19] for the second layer. All heavy atoms were frozen in crystallographic positions. The obtained clusters were used for energy calculations. Two-body interaction energy (ΔE^2) was defined as the energy difference between the energy of the dimer and the sum of monomer energies.

$$\Delta E^2(AB) = E(AB) - E(A) - E(B) \quad (1)$$

Three-body energy (ΔE^3) was defined as the energy difference between the total energy of the trimer and the sum of both monomer energies and all ΔE^2 values.

$$\Delta E^3(ABC) = E(ABC) - E(A) - E(B) - E(C) - \Delta E^2(AB) - \Delta E^2(BC) - \Delta E^2(AC) \quad (2)$$

Expanding the ΔE^2 energies, the $\Delta E^3(ABC)$ could thus be expressed as:

$$\Delta E^3(ABC) = E(ABC) - E(AB) - E(AC) - E(BC) + E(A) + E(B) + E(C) \quad (3)$$

The sum of the ΔE^2 values ($\sum \Delta E^2(A)$) of the central molecule A was computed for residues in the first and second layers. The whole layers were labeled as Q and were formed by residues marked as B to N).

$$\sum E^2(A) = \sum_{I=B}^N E^2(AI) \quad (4)$$

Finally, the interaction of the central molecule A with the surrounding molecules was computed as:

$$\Delta E(AQ) = E(AQ) - E(A) - E(Q) \quad (5)$$

The many-body energy (ΔE^{MB}) was computed as the difference $\Delta E(AQ)$ and $\sum \Delta E^2(A)$.

$$\Delta E^{MB}(AQ) = \Delta E(AQ) - \sum \Delta E^2(A) \quad (6)$$

The energies were determined using the DFT-D3 method with the Tao, Perdew, Staroverov and Scuseria (TPSS) functional and the triple-zeta TZVPP basis set. Three-body dispersion was not used for the TPSS functional because it had been shown that the ΔE^3 of TPSS was too repulsive and the three-body dispersion only made the overall errors worse [20]. The benchmark ΔE^2 were determined by the MP2.5 method [21] with the complete basis set (CBS). MP2.5/CBS was calculated as the sum of the Møller–Plesset perturbation theory to the second order (MP2) with CBS and the scaled third-order energy contribution (the scaling factor of 0.5) using the augmented correlation-consistent polarized double-zeta (aug-cc-pVDZ) basis set. For MP2/CBS, an extrapolation from aug-cc-pVDZ to aug-cc-pVTZ was used [22]. Counterpoise corrections for the basis set superposition error (BSSE) and RI approximations were used for the MP2.5 calculations. ΔE^2 values were decomposed by symmetry-adapted perturbation-theory (SAPT) methodology. The simplest truncation of SAPT (SAPT0) decomposition [23] was performed with the recommended jun-cc-pVDZ basis sets (i.e. cc-pVDZ on hydrogen and aug-cc-pVDZ on heavier atoms) [24]. Turbomole (7.0) [25], P_{S1}4 [26], MOPAC2016 [27] and Cuby4 [28] were used.

3. Results and Discussion

3.1. The Properties of Isolated Molecules

To obtain a deeper insight into the noncovalent interactions of phosphaboranes, we computed the ESP surfaces of **1** and **2** and compared them with analogous compounds in the literature. The parent *closo*-1,2- $P_2B_{10}H_{10}$ compound was reported to have highly positive σ -holes with a magnitude ($V_{S,max}$) of 22.6 kcal mol⁻¹ and a large dipole moment of 2.7 D [8]. The introduction of two electronegative Cl atoms in compound **1** resulted in even more positive σ -holes ($V_{S,max}$ of about 25.2 kcal mol⁻¹, see Figure 2 and Table 1). The dipole moment of **1** was, however, smaller (1.2 D) because the vector addition of the two B–Cl bond dipole moments [29] was in the opposite direction with respect to the vector pointing out from the midpoint of the P(1)–P(2) vector towards the center of the cluster. The Cl atoms of **1** had slightly positive σ -holes ($V_{S,max}$ 2.3 kcal mol⁻¹) and the minimum value of the ESP molecular surface ($V_{S,min}$) of the Cl(3,6) atom was -9.5 kcal mol⁻¹. The Cl atoms of **1** are thus expected to be better H-bond acceptors than X-bond donors.

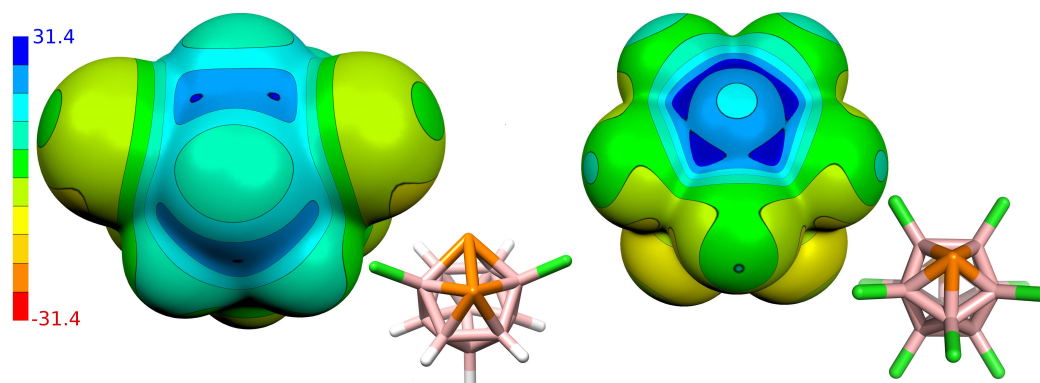


Figure 2. The computed molecular electrostatic potential (ESP) surface and molecular diagrams for 3,6-Cl₂-*closo*-1,2- $P_2B_{10}H_8$ and *closo*-1,7- $P_2B_{10}Cl_{10}$; the color range of the ESP in kcal mol⁻¹.

Table 1. The magnitudes of the σ -holes ($V_{S,max}$) of the P and Cl atoms.

Compound	Atom	$V_{S,max}$ [kcal mol ⁻¹]
3,6-Cl ₂ - <i>closo</i> -1,2-P ₂ B ₁₀ H ₈ (1)	P(1,2)	2 × 25.2; 25.1
	Cl(3,6) ¹	2.3
<i>closo</i> -1,7-P ₂ B ₁₀ Cl ₁₀ (2)	P(1,7)	30.2; 2 × 28.9; 2 × 27.8
	Cl(2,3)	13.1
	Cl(9,10) ²	1.5

¹ The minimum value of the electrostatic potential (ESP) molecular surface of the Cl(3,6) atom is -9.5 kcal mol⁻¹. ² The minimum value of the ESP molecular surface of the Cl(9,10) atom is -13.2 kcal mol⁻¹.

A complete substitution of terminal hydrogens by chlorines considerably increased the dipole moment to 3.4 D (eight B–Cl bond dipole moments were added to the vector from the P(1)–P(7) midpoint towards the center of the cluster) and $V_{S,max}$ values up to 30.2 kcal mol⁻¹ in the case of **2**. It can thus be considered as a very good Pn-bond donor. Additionally, the Cl(2,3) atoms of **2** had positive σ -holes with a $V_{S,max}$ value of 13.1 kcal mol⁻¹; the $V_{S,min}$ of the Cl(9,10) atoms was -13.2 kcal mol⁻¹. Therefore, the Cl atoms of **2** can act as both X-bond donors and H-bond acceptors.

3.2. Interactions in the Single Crystal of **1** and the Crystal of **2**•Toluene

Initially, the crystal structure of **1** was analyzed. There are eight molecules in the unit cell (see Figure 3). First, all pairwise interactions were evaluated by computing interaction energy (ΔE^2) values by the DFT-D3 method using various functionals and basis sets. For the most stable motifs, highly accurate MP2.5/CBS ΔE^2 values were computed. Additionally, ΔE^2 was decomposed into different terms by using the SATP technique. The obtained results are summarized in Table 2. The SAPT0/jun-cc-pVDZ results were in reasonable agreement with the MP2.5/CBS results (the root-mean-square error (RMSE) of 0.41 kcal mol⁻¹). Among the DFT-D3 methods, the best agreement with MP2.5/CBS results, i.e. the RMSE of 0.47 kcal mol⁻¹, was found for the TPSS/TZVPP level. The other tested functionals and basis sets had a bigger RMSE, i.e. 1.31, 1.29, 1.19 and 1.10 kcal mol⁻¹ for BLYP/def2-QZVP, BLYP/DZVP, B3LYP/DZVP and TPSS/DZVP, respectively. The ΔE^2 values ranged from -3.35 to -4.23 kcal mol⁻¹ at the MP2.5/CBS level. These values are large considering that there were no intermolecular distances shorter than the sum of van der Waals radii (Σr_{vdW}) [30] in the crystal. The highly negative ΔE^2 values were caused by the large dispersion contribution, which strongly dominated the interaction (65–71% of the total attractive energy). The electrostatic interaction was also important (21–27% of the total attractive energy). The smallest attractive term was induction (7–8% of the total attractive energy).

Table 2. Computed DFT-D3/TPSS/TZVPP and MP2.5/CBS two-body interaction energies for the crystal of 3,6-Cl₂-*closo*-1,2-P₂B₁₀H₈ (**1**). Interaction energies were decomposed into electrostatic (E_{elec}), induction (E_{ind}), dispersion (E_{disp}), and exchange (E_{exch}) contributions by SAPT0. Energies in kcal mol⁻¹. The relative values in parentheses express the contribution to the sum of all attractive energy terms of SAPT0.

Interaction	DFT-D3/MP2.5	SAPT0/jun-cc-pVDZ				
		Total	E_{elec}	E_{ind}	E_{disp}	E_{exch}
A...B	-4.85/-4.23	-4.83	-2.28 (21%)	-0.81 (8%)	-7.67 (71%)	5.94
A...C	-4.09/-3.90	-4.01	-2.26 (27%)	-0.61 (7%)	-5.42 (65%)	4.28
A...D	-3.85/-3.35	-3.70	-2.11 (24%)	-0.65 (8%)	-5.87 (68%)	4.92

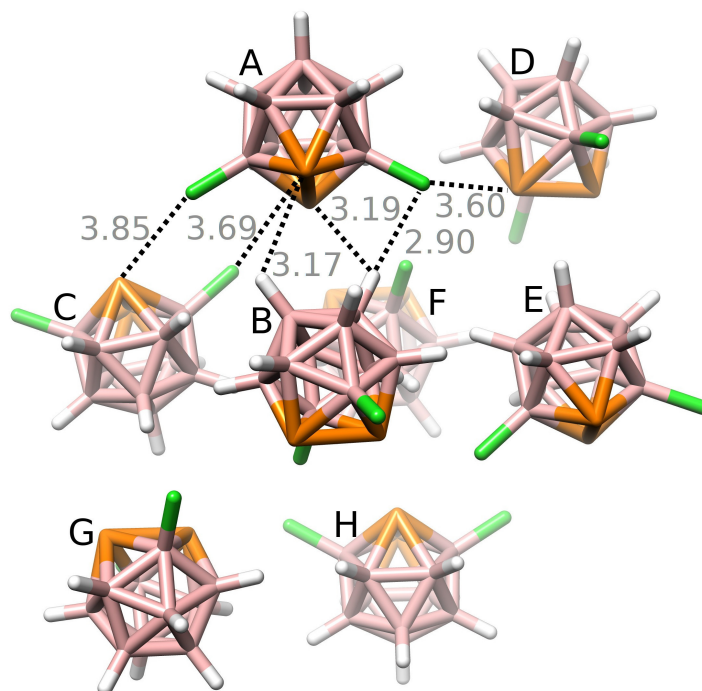


Figure 3. The crystal packing of 3,6-Cl₂-closo-1,2-P₂B₁₀H₈ (**1**). Distances in Å. The color gray is used for distances larger than Σr_{vdW} . The positions of H atoms were optimized at the DFT-D3/BLYP/DZVP level.

The sum of ΔE^2 values ($\Sigma \Delta E^2(\mathbf{1})$) was $-48.45 \text{ kcal mol}^{-1}$ for the first layer. The consideration of the second layer made the $\Sigma \Delta E^2(\mathbf{1})$ more negative by $3.38 \text{ kcal mol}^{-1}$. Three-body energy $\Delta E^3(ABC)$, $\Delta E^3(ACD)$ and $\Delta E^3(BCD)$ values were relatively small (below 2% of ΔE^2). They ranged from -0.01 to $0.22 \text{ kcal mol}^{-1}$ at the DFT-D3/TPSS/TZVPP level. Similar ΔE^3 results were obtained at the DFT-D3/B3LYP/DZVP level (ΔE^3 ranged from -0.05 to $0.14 \text{ kcal mol}^{-1}$).

Secondly, we studied interactions in the crystal of **2**•toluene. The results showed that the most negative ΔE^2 value was exhibited by the B-P $\cdots\pi$ Pn-bond. The Pn-bond was characterized by a small length of 3.08 \AA (88% of Σr_{vdW}) and its ΔE^2 value exceeded $-10 \text{ kcal mol}^{-1}$ at the MP2.5/CBS level (see Table 3 and Figure 4). The SAPT decomposition revealed that electrostatic and induction contributions were more important in this Pn-bond. They represented 35% and 14% of the total attractive energy of this Pn-bond, respectively, but they did not exceed 27% and 10% of the total attractive energy in the other interactions reported in this study. Pn $\cdots\pi$ interactions in neutral complexes are well known, especially for heavier Pn atoms (As, Sb and Bi). For example, AsCl₃ and SbCl₃ formed Pn $\cdots\pi$ Pn-bonds with substituted benzenes that had a Pn \cdots benzene_{centroid} separation of 3.14 and 3.24 \AA (88 and 86% of Σr_{vdW}), respectively [31,32]. Phosphorus $\cdots\pi$ interactions are typically only observed in cationic phosphorus complexes, as exemplified by the interaction between the Mes⁺NP⁺ cation and benzene, which has a P \cdots benzene_{centroid} separation of 3.00 \AA (86% of Σr_{vdW}) [33]. The reported Pn-bond can be further related to analogous σ -hole interactions in heteroboranes. For example, the C-Br $\cdots\pi$ chalcogen bond reported for brominated carboranes had a length of 3.46 \AA (98% of Σr_{vdW}) [34] and the ΔE value of the isolated X-bond was estimated to be about -4 kcal mol^{-1} [11]. The B-S $\cdots\pi$ chalcogen bond found in phenyl-substituted thiaboranes had a length of 3.24 \AA (93% of Σr_{vdW}) and a ΔE of $-8.6 \text{ kcal mol}^{-1}$ [9]. The Sb₂ \cdots H-B Pn-bond with a length of 2.78 \AA (88% of Σr_{vdW}) and a ΔE^2 of $-6.46 \text{ kcal mol}^{-1}$ was found in the single crystal of the stibacarbaborane molecule [12]. The ΔE^2 values of hypothetical *closo*-1,2-P₂B₁₀H₁₀ \cdots benzene, *closo*-1,2-As₂B₁₀H₁₀ \cdots benzene, and AsCl₃ \cdots benzene Pn-bonded complexes were computed and reported to be -4.8 , -5.6 and $-6.5 \text{ kcal mol}^{-1}$, respectively [8,35].

The computed $\sum \Delta E^2$ values were used to evaluate the importance of the B-P $\cdots\pi$ Pn-bond for the crystal packing of **2**•toluene. The $\sum \Delta E^2(\text{toluene})$ and $\sum \Delta E^2(\mathbf{2})$ were -31.55 and -57.12 kcal mol $^{-1}$ for the first layer, respectively. The B-P $\cdots\pi$ Pn-bonds thus formed 63 and 35 % of $\sum \Delta E^2(\text{toluene})$ and $\sum \Delta E^2(\mathbf{2})$, respectively. The consideration of the second layer made $\sum \Delta E^2(\text{toluene})$ and $\sum \Delta E^2(\mathbf{2})$ more negative by about 1.98 and 5.13 kcal mol $^{-1}$, which lowered the relative contribution of Pn-bonds to 60% and 32%, respectively. Additionally, the computed ΔE^3 values of the Pn-bonds were more repulsive than for those of the other interactions. The $\Delta E^3(\mathbf{2}\text{toluene}\mathbf{2})$ and $\Delta E^3(\text{toluene}\mathbf{2}\text{toluene})$ sandwich-like motifs stabilized by the Pn-bond were 1.34 and 0.36 kcal mol $^{-1}$, respectively, at the DFT-D3/TPSS/TZVPP level. The ΔE^3 thus further reduced the strength of the Pn-bonding by about 7%. The other interactions were reduced by less than 2% by the ΔE^3 . The role of many-body energies was further examined by computing the ΔE^{MD} for the toluene cluster (the first layer considered). The obtained value of 2.64 kcal mol $^{-1}$ represented 8% of the $\sum \Delta E^2(\text{toluene})$ value. Summarizing the results shown above, the Pn-bond formed about 56 and 32% of the computed binding energy for the toluene and **2**, respectively. These results indicate the large importance of Pn-bonding, especially for toluene. Interestingly, the diX-bonds represented about 42% of the computed binding of **2**, which was even more than that of Pn-bonding in this case. Even though the diXbonds were considerably weaker than the Pn-bonds (see Table 3), they were much more numerous, which resulted in an overall large contribution to the computed binding energy.

Table 3. Computed DFT-D3/TPSS/TZVPP and MP2.5/CBS two-body interaction energies for the crystal of *closo*-1,7-P₂B₁₀Cl₁₀(**2**)•toluene. Interaction energies were decomposed into electrostatic (E_{elec}), induction (E_{ind}), dispersion (E_{disp}), and exchange (E_{exch}) contributions by SAPT0. Energies in kcal mol $^{-1}$. The relative values in parentheses express the contribution to the sum of all attractive energy terms of SAPT0.

Interaction	DFT-D3/MP2.5	SAPT0/jun-cc-pVDZ				
		Total	E_{elec}	E_{ind}	E_{disp}	E_{exch}
2 \cdots toluene Pn-bond	−9.94/−10.55	−11.56	−9.80 (35%)	−3.96 (14%)	−14.61 (52%)	16.81
2 \cdots toluene stacking	−2.51/−2.25	−1.96	−0.84 (22%)	−0.21 (6%)	−2.75 (72%)	1.84
2 \cdots toluene H-bond	−0.87/−0.80	−0.51	−0.35 (16%)	−0.21 (10%)	−1.58 (74%)	1.63
2 \cdots 2 bifurcated diX-bonds	−3.67	−3.27	−1.17 (16%)	−0.32 (4%)	−5.73 (79%)	3.95
2 \cdots 2 bifurcated diX-bond	−2.94	−3.01	−1.78 (26%)	−0.40 (6%)	−4.67 (68%)	3.84
2 \cdots 2 diX-bond	−2.32/−2.65	−2.13	−1.51 (25%)	−0.35 (6%)	−4.13 (69%)	3.86

The shortest intermolecular Cl \cdots Cl separation in the crystal structure was 3.38 Å (96% of Σr_{vdW}). The diX-bond had ΔE^2 of -2.65 kcal mol $^{-1}$ at the MP2.5/CBS level. The geometrical arrangement of this interaction had very similar Θ_1 and Θ_2 angles (i.e. B-Cl \cdots Cl angles of 125° and 127°), which is typical of diX-bonds [36]. Additionally, H-bonding can also be found in the crystal of **2**•toluene. The H-bond had the least negative ΔE^2 value among the interaction motifs in this study and the H \cdots Cl distance was 2.74 Å (96% of Σr_{vdW}).

In summary, we analyzed noncovalent interactions in the single crystal of **1** and in the crystal of **2**•toluene by quantum chemical protocols. The analysis revealed numerous diXbonds and unusually strong B-P $\cdots\pi$ pnictogen bonds, which dominated the crystal packing of the crystal of **2**•toluene. The Pn-bond length was significantly below Σr_{vdW} and the ΔE value overcoming -10 kcal mol $^{-1}$.

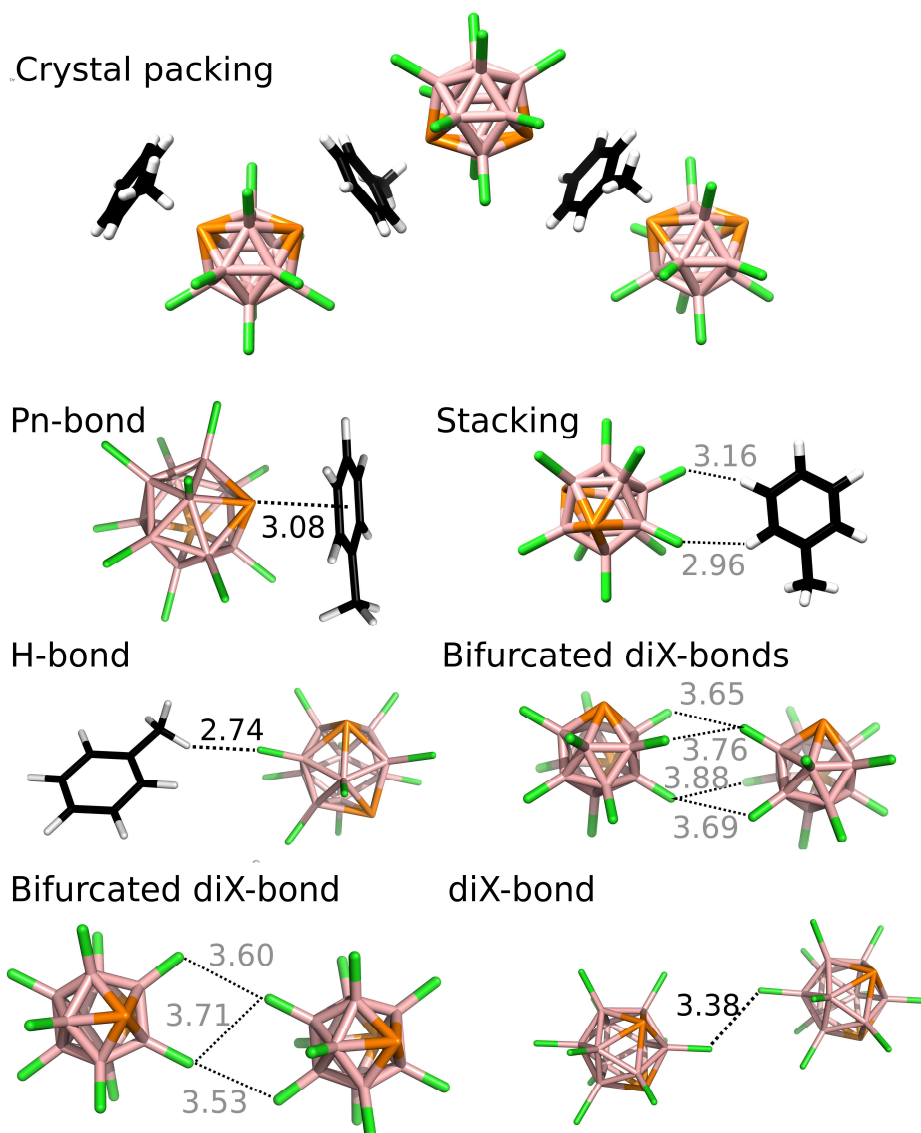


Figure 4. The crystal packing and binding motifs of *closo*-1,7- $P_2B_{10}Cl_{10}$ •toluene. Distances in Å. The color gray is used for distances larger than Σr_{vdW} . The positions of H atoms were optimized at the DFT-D3/BLYP/DZVP level.

Author Contributions: Methodology, J.F. and D.H.; Writing Draft Preparation, J.F. and D.H.; Visualization, J.F.; Project Administration, J.F. and D.H.

Funding: This work was supported by the research project RVO 61388963 of the Czech Academy of Sciences. This research was funded by the Czech Science Foundation grant number 17-08045S.

Conflicts of Interest: The authors declare no conflicts of interest.

References

1. Grüner, B.; Hnyk, D.; Císařová, I.; Plzák, Z.; Štíbr, B. Phosphaborane Chemistry. Syntheses and Calculated Molecular Structures of Mono- and Di-chloro Derivatives of 1,2-Diphospha-*closo*-dodecaborane(10). *J. Chem. Soc. Dalton Trans.* **2002**, *15*, 2954–2959. [[CrossRef](#)]
2. Štíbr, B.; Holub, J.; Bakardjiev, M.; Hnyk, D.; Tok, O.L.; Milius, W.; Wrackmeyer, B. Phosphacarborane Chemistry: The Synthesis of the Parent Phosphadecaboranes *nido*-7,8,9- $PC_2B_8H_{11}$ and [*nido*-7,8,9- $PC_2B_8H_{10}$][−], and Their 10-Cl Derivatives—Analogues of the Cyclopentadiene Anion. *Eur. J. Inorg. Chem.* **2002**, *9*, 2320–2326. [[CrossRef](#)]

3. Little, J.L.; Whitesell, M.A.; Chapman, R.W.; Kester, J.G.; Huffman, J.C.; Todd, L.J. Synthesis of Some 10-, 11-, and 12-Atom Phosphaboranes. Crystal Structure of 2-(Trimethylamine)-1-PB₁₁H₁₀. *Inorg. Chem.* **1993**, *32*, 3369–3372. [[CrossRef](#)]
4. Keller, W.; Sawitzki, G.; Haubold, W. Synthesis of Halogenated Polyhedral Phosphaboranes. Crystal Structures of *closo*-1,7-P₂B₁₀Cl₁₀. *Inorg. Chem.* **2000**, *39*, 1282–1287. [[CrossRef](#)] [[PubMed](#)]
5. Melichar, P.; Hnyk, D.; Fanfrlík, J. Systematic Examination of Classical and Multi-Center Bonding in Heteroborane Clusters. *Phys. Chem. Chem. Phys.* **2018**, *20*, 4666–4675. [[CrossRef](#)] [[PubMed](#)]
6. Hnyk, D.; Všetěčka, V.; Drož, L.; Exner, O. Charge Distribution within 1,2-Dicarba-*closo*-dodecaborane: Dipole Moments of its Phenyl Derivatives. *Collect. Czech. Chem. Commun.* **2001**, *66*, 1375–1379. [[CrossRef](#)]
7. Clark, T.; Hennemann, M.; Murray, J.S.; Politzer, P. Halogen Bonding: The σ -Hole. *J. Mol. Model.* **2007**, *13*, 291–296. [[CrossRef](#)] [[PubMed](#)]
8. Pecina, A.; Lepšík, M.; Hnyk, D.; Hobza, P.; Fanfrlík, J. Chalcogen and Pnictogen Bonds in Complexes of Neutral Icosahedral and Biccaped Square-Antiprismatic Heteroboranes. *J. Phys. Chem. A* **2015**, *119*, 1388–1395. [[CrossRef](#)] [[PubMed](#)]
9. Fanfrlík, J.; Páda, A.; Padělková, Z.; Pecina, A.; Macháček, J.; Lepšík, M.; Holub, J.; Růžička, A.; Hnyk, D.; Hobza, P. The Dominant Role of Chalcogen Bonding in the Crystal Packing of 2D/3D Aromatics. *Angew. Chem. Int. Ed.* **2014**, *53*, 10139–10142. [[CrossRef](#)] [[PubMed](#)]
10. Fanfrlík, J.; Hnyk, D. Chalcogens Act as Inner and Outer Heteroatoms in Borane Cages with Possible Consequences for σ -Hole Interactions. *CrystEngComm* **2016**, *47*, 8973–9162. [[CrossRef](#)]
11. Fanfrlík, J.; Holub, J.; Růžičková, Z.; Řezáč, J.; Lane, P.D.; Wann, D.A.; Hnyk, D.; Růžička, A.; Hobza, P. Competition between Halogen, Hydrogen and Dihydrogen Bonding in Brominated Carboranes. *ChemPhysChem* **2016**, *17*, 3373–3376.
12. Holub, J.; Melichar, P.; Růžičková, Z.; Vrána, J.; Wann, D.A.; Fanfrlík, J.; Hnyk, D.; Růžička, A. A Novel Stibacarbaborane Cluster with Adjacent Antimony Atoms Exhibiting Unique Pnictogen Bond Formation that Dominates Its Crystal Packing. *Dalton Trans.* **2017**, *46*, 13714–13719. [[CrossRef](#)] [[PubMed](#)]
13. Holub, J.; Růžičková, Z.; Hobza, P.; Fanfrlík, J.; Hnyk, D.; Růžička, A. Various Types of Non-covalent Interactions Contributing Towards Crystal Packing of Halogenated Diphospha-dicarborene with an Open Pentagonal Belt. *New J. Chem.* **2018**, *42*, 10481–10483. [[CrossRef](#)]
14. Frisch, M.J.; Trucks, G.W.; Schlegel, H.B.; Scuseria, G.E.; Robb, M.A.; Cheeseman, J.R.; Scalmani, G.; Barone, V.; Mennucci, B.; Petersson, G.A.; et al. *Gaussian 09, Revision, D.01*; Gaussian, Inc.: Wallingford, CT, USA, 2009.
15. Flückiger, P.; Lüthi, H.P.; Portmann, S.; Weber, J. MOLEKEL 4.3; Swiss Center for Scientific Computing; Manno, Switzerland, 2000.
16. Portmann, S.; Lüthi, H.P. MOLEKEL: An Interactive Molecular Graphic Tool. *CHIMIA Int. J. Chem.* **2000**, *54*, 766–770.
17. Riley, K.E.; Tran, K.A.; Lane, P.; Murray, J.S.; Politzer, P. Comparative Analysis of Electrostatic Potential Maxima and Minima on Molecular Surfaces, as Determined by Three Methods and a Variety of Basis Sets. *J. Comput. Sci.* **2016**, *17*, 273–284. [[CrossRef](#)]
18. Hostaš, J.; Řezáč, J. Accurate DFT-D3 Calculations in a Small Basis Set. *J. Chem. Theory Comput.* **2017**, *13*, 3575–3585. [[CrossRef](#)] [[PubMed](#)]
19. Řezáč, J.; Hobza, P. Advanced Corrections of Hydrogen Bonding and Dispersion for Semiempirical Quantum Mechanical Methods. *J. Chem. Theory Comput.* **2012**, *8*, 141–151. [[CrossRef](#)] [[PubMed](#)]
20. Řezáč, J.; Huang, Y.; Hobza, P.; Beran, J.O.G. Benchmark Calculations of Three-Body Intermolecular Interactions and the Performance of Low-Cost Electronic Structure Methods. *J. Chem. Theory Comput.* **2015**, *11*, 3065–3079. [[CrossRef](#)] [[PubMed](#)]
21. Pitonak, M.; Neogady, P.; Cerny, J.; Grimme, S.; Hobza, P. Scaled MP3 Non-Covalent Interaction Energies Agree Closely with Accurate CCSD(T) Benchmark Data. *ChemPhysChem* **2009**, *10*, 282–289. [[CrossRef](#)] [[PubMed](#)]
22. Halkier, A.; Helgaker, T.; Jørgensen, P.; Klopper, W.; Koch, H.; Olsen, J.; Wilson, A.K. Basis-Set Convergence in Correlated Calculations on Ne, N₂, and H₂O. *Chem. Phys. Lett.* **1998**, *286*, 243–252. [[CrossRef](#)]
23. Jeziorski, B.; Moszynski, R.; Szalewicz, K. Perturbation Theory Approach to Intermolecular Potential Energy Surfaces of van der Waals Complexes. *Chem. Rev.* **1994**, *94*, 1887–1930. [[CrossRef](#)]

24. Parker, T.M.; Burns, L.A.; Parrish, R.M.; Ryno, A.G.; Sherrill, C.D. Levels of Symmetry Adapted Perturbation Theory (SAPT). I. Efficiency and Performance for Interaction Energies. *J. Chem. Phys.* **2014**, *140*, 094106. [[CrossRef](#)] [[PubMed](#)]
25. Ahlrichs, R.; Bar, M.; Haser, M.; Horn, H.; Kolmel, C. Electronic Structure Calculations on Workstation Computers: The Program System Turbomole. *Chem. Phys. Lett.* **1989**, *162*, 165–169. [[CrossRef](#)]
26. Turney, J.M.; Simmonett, A.C.; Parrish, R.M.; Hohenstein, E.G.; Evangelista, F.; Fermann, J.T.; Mintz, B.J.; Burns, L.A.; Wilke, J.J.; Abrams, M.L.; et al. Psi4: An Open-Source Ab Initio Electronic Structure Program. *WIREs Comput. Mol. Sci.* **2012**, *2*, 556–565. [[CrossRef](#)]
27. Stewart, J.P. Optimization of parameters for semiempirical methods IV: Extension of MNDO, AM1, and PM3 to more main group elements. *J. Mol. Model.* **2004**, *10*, 155–164. [[CrossRef](#)] [[PubMed](#)]
28. Řezáč, J. Cuby: An Integrative Framework for Computational Chemistry. *J. Comput. Chem.* **2016**, *37*, 1230–1237. [[CrossRef](#)] [[PubMed](#)]
29. Macháček, J.; Plešek, J.; Holub, J.; Hnyk, D.; Všecká, V.; Císařová, I.; Kaupp, M.; Štíbr, B. New Route to 1-Thia-closo-dodecaborane(11), closo-1-SB₁₁H₁₁, and Its Halogenation Reactions. The Effect of the Halogen on the Dipole Moments and the NMR Spectra and the Importance of Spin-Orbit Coupling for the ¹¹B Chemical Shifts. *Dalton Trans.* **2006**, 1024–1029.
30. Mantina, M.; Chamberlin, A.C.; Valero, R.; Cramer, C.J.; Truhlar, D.G. Consistent van der Waals Radii for the Whole Main Group. *J. Phys. Chem. A* **2009**, *113*, 5806–5812. [[CrossRef](#)] [[PubMed](#)]
31. Schmidbaur, H.; Nowak, R.; Steigelmann, O.; Muller, G. π -Complexes of p-Block Elements: Synthesis and Structures of Adducts of Arsenic and Antimony Halides with Alkylated Benzenes. *Chemische Berichte* **1990**, *123*, 1221–1226. [[CrossRef](#)]
32. Burford, N.; Clyburne, J.A.C.; Wiles, J.A.; Cameron, T.S.; Robertson, K.N. Tethered Diarenes as Four-Site Donors to SbCl₃. *Organometallics* **1996**, *15*, 361–364. [[CrossRef](#)]
33. Burford, N.; Clyburne, J.A.C.; Bakshi, P.K.; Cameron, T.S. η^6 -Arene Complexation to a Phosphenium Cation. *J. Am. Chem. Soc.* **1993**, *115*, 8829–8830. [[CrossRef](#)]
34. McGrath, T.D.; Welch, A.J. Steric Effects in Heteroboranes. IV. 1-Ph-2-Br-1,2-closo-C₂B₁₀H₁₀. *Acta Cryst.* **1995**, *C51*, 649–651. [[CrossRef](#)]
35. Bauzá, A.; Quiñero, D.; Deyà, P.M.; Frontera, A. Halogen Bonding versus Chalcogen and Pnictogen Bonding: A Combined Cambridge Structural Database and Theoretical Study. *CrystEngComm* **2013**, *15*, 3137–3144. [[CrossRef](#)]
36. Awwadi, F.F.; Willet, R.D.; Peterson, K.A.; Twamley, B. The Nature of Halogen···Halogen Synthons: Crystallographic and Theoretical Studies. *Chem. Eur. J.* **2006**, *12*, 8952–8960. [[CrossRef](#)] [[PubMed](#)]



© 2018 by the authors. Licensee MDPI, Basel, Switzerland. This article is an open access article distributed under the terms and conditions of the Creative Commons Attribution (CC BY) license (<http://creativecommons.org/licenses/by/4.0/>).